Unusual Photon Tunneling Caused by Negative Refraction

Qing Hao
Department of Mechanical Engineering
Massachusetts Institute of Technology

Abstract

In recent years, tremendous efforts have been devoted to a class of novel metamaterials, left-handed materials (LHMs), which reverse the behavior of many fundamental electromagnetic properties associated with materials. In this investigation, we briefly discuss the application of LHMs in enhancing photon tunneling, which is used in thermophotovoltaic devices and scanning photon-tunneling microscopy.

1. Introduction

As one of the most fundamental phenomena in optics, refraction has been studied for a long time. In the nature, all known materials exhibit positive refractive indices. When a light beam crosses the interface between two positive index media (PIM), it will be bent positively, i.e., on the opposite side of the normal to the interface. Furthermore, the Snell's law dictates that $n_1 \sin\theta_1 = n_2 \sin\theta_2$, where θ_1 is the angle subtended between the incident ray and the normal, θ_2 is the included angle between the refracted ray and the normal, n_1 and n_2 are the refractive indices of media 1 and 2, respectively.

Regarded as a common sense by many people, the above knowledge was challenged after the discovery of negative index media (NIM). In 1968, Soviet physicist Victor Veselago first hypothesized the existence of such materials with simultaneous negative permittivity ε and permeability μ, resulting in an effective negative index of refraction, $n = \sqrt{\mu}\sqrt{\varepsilon}$ [1]. Opposite to PIM, the triplet set of vectors $\vec{E}$, $\vec{H}$, $\vec{k}$ in NIM is left-handed, and thus they are also called left-handed materials (LHMs). When a ray of light passes the PIM-NIM interface, it will be bent negatively according to the Snell's law. Due to the negative ε, μ, and n values, other fundamental phenomena such as the Doppler effect, Cerenkov radiation, anomalous refraction, and radiation pressure will also be reversed [2, 3].

Although little attention was paid to LHMs for almost thirty years, it has become a frequently mentioned topic recently since the practical realization of LH materials with split ring resonators (SRRs) and thin-wire structures were demonstrated [3, 4]. The first experimental realization based on microwave scattering was accomplished in 2001 [5]. Although divergent views were held on the explanation of the experimental data and its theoretical foundation was also questioned [6, 7], negative refraction has recently been reconfirmed in both experiments and theories [8-12]. For applications, research is actively conducted on a perfect lens [2] and unusual photon tunneling phenomena [13].

In this paper, we investigate the possibilities of using LHMs to enhance the photon tunneling through a vacuum gap. Our discussion will focus on thermophotovoltaic devices and scanning photon-tunneling microscopy. The paper is divided into three sections. The first section briefly introduces the idea of using LHMs to amplify evanescent waves in a perfect lens. The second section demonstrates this idea based on

calculations employing a transfer matrix method. Finally, future work in this area is discussed according to several recent advancements.

2. Amplifying Evanescent Waves Using LHMs

One important application of NIM is a perfect lens, or a "superlens." As an unconventional alternative to a lens, NIM can focus light even in the form of a parallel-sided slab of material (Fig. 1). The reason lies in the negative wave vector $k_z' = -\sqrt{\omega^2 c^{-2} - k_x{}^2 - k_y{}^2}$ in the z direction, whereas we have $k_z = \sqrt{\omega^2 c^{-2} - k_x{}^2 - k_y{}^2}$ for PIM [1]. In a perfect lens, the transmission coefficient has a reversed phase

$$T = \exp\left(ik_z' d\right) = \exp\left(-i\sqrt{\omega^2 c^{-2} - k_x{}^2 - k_y{}^2}\, d\right). \quad (1)$$

This phase reversal compensates the phase difference between different paths of the focused rays. The slab "undoes" the effect of a vacuum with the same thickness, and behaves like optical antimatter [14].

Image removed due to copyright considerations. See reference [2].

Fig. 1. A negative refractive index medium bends light to a negative angle with the surface normal. Released from the medium, the light reaches a focus for a second time. [2].

Remarkably, a perfect lens can also cancel the decay of evanescent waves, which represent Fourier components with $k_x{}^2 + k_y{}^2 > \omega^2 c^{-2}$ [2]. Since both propagating and evanescent waves will contribute to the image resolution, a perfect lens can focus an image with a resolution unrestricted by the wavelength of light. This will lead to ultra-high-capacity DVDs and smaller, faster computer chips. In a conventional lens, an evanescent wave, with an imaginary wave vector

$$k_z = i\sqrt{k_x{}^2 + k_y{}^2 - \omega^2 c^{-2}}, \quad k_x{}^2 + k_y{}^2 > \omega^2 c^{-2}, \quad (2)$$

will exponentially decay along the distance and have a negligible amplitude before reaching the image plane (Fig. 2(a)). In contrast, in a perfect lens the evanescent waves can be amplified exponentially in the lens (Fig. 2(b)). This does not violate energy conservation because evanescent waves transport no energy [2]. For both S-polarized light and P-polarized light, the evanescent waves have transmission coefficient

$$\lim_{\mu,\varepsilon\to -1} T = \exp\left(d\sqrt{k_x{}^2 + k_y{}^2 - \omega^2 c^{-2}}\right), \quad (3)$$

which is derived by summing up the multiple scattering events [2].

Fig. 2. (a) The missing components of the image are contained in the near field that decays exponentially and makes negligible contribution to the image. (b) A perfect lens has the capacity to amplify the near field so that it contributes to the image, thus removing the wavelength limitation [14].

Despite the simple form of Eq. (3), problems will arise when we consider the extreme cases in which $z \to \infty$ for evanescent waves and $z \to -\infty$ for incident and reflected waves. To avoid infinity, it was suggested that the definitions of electrical fields E^i, E^t should be restricted to a finite region, beyond which the transmission coefficient t becomes zero [15]. In this paper, we will avoid using semi-infinite LHM regions and limit the LHM layer thickness to several wavelengths.

3. Unusual Photon Tunneling in the Presence of a LHM Layer

When the incident angle of a light beam is greater than the critical angle from an optically denser material to another material, total internal reflection will occur in the first medium. Although no energy is transferred by refraction, evanescent waves decay exponentially from the interface into the second medium. When a third medium with sufficiently large refractive index is placed behind a thin slab of the second material, photons can tunnel through the second medium into the third one. This phenomenon, called photon tunneling, has been used in attenuated total reflectance spectroscopy and scanning photon tunneling microscopy [13]. Recently, microscale thermophotovoltaic devices using photon tunneling have been proposed to enhance the radiative transfer, hence increasing the energy conversion efficiency [16].

To obtain significant photon tunneling, the distance between the receiving surface and the emitting surface should be much less than the characteristic wavelength. Using NIM to amply the amplitudes of evanescent waves, this distance can be greatly increased. Based on a multilayered structure with semi-infinite top and bottom PIM layer, an unusual photon tunneling through the combined PIM and NIM is suggested by calculation [13]. This may have an impact on applications such as microscale thermophotovoltaic devices.

In this section, our discussion will concentrate on the above two applications of unusual photon tunneling: thermophotovoltaic devices and scanning photon-tunneling microscopy.

3.1 Introduction to Thermophotovoltaic Devices

The maximum amount of heat intensity that can be transferred by radiation from a black body of refractive index n_{BB} to an adjacent object with refractive index n_{OBJ} is shown to be the square of $\min\{n_{BB}, n_{OBJ}\}$ times the free space Planck distribution [16], which implies that the radiative power spectral density within a thermophotovoltaic cell could be designed to be much greater than the free space Planck distribution. This phenomena, called the "spacing effect," or microscale radiative transfer, results from black body modes that are evanescent in the space between the black body and the object.

Images removed due to copyright considerations.
See references [16] and [13].

Fig. 3. (a) Radiation from within the black body (labeled "BB" or medium "1") is incident on the surface of the black body at an angle θ_i measured from the normal direction z [16]. (b) Schematic of a multilayered system [13].

Fig. 3 (a) presents an object separated from a blackbody by a vacuum gap with a thickness L. As mentioned, the blackbody power spectral density in an optical medium of index n_{BB} is larger than that in the free space by a factor of ${n_{BB}}^2$ ($n_{BB} \le n_{OBJ}$)

$$W_{solid}(\omega)\,d\omega d\Omega = {n_{BB}}^2 \frac{\hbar\omega}{\exp(\hbar\omega/k_B T_{BB})-1}\frac{\omega^2 d\omega d\Omega}{(2\pi)^3 c^2}, \tag{4}$$

which is due to the fact that photon density of states is increased to ${n_{BB}}^3 d^3k$ and the speed of light is decreased to c/n_{BB} in the blackbody. Without tunneling, only propagating modes, which are incident on the interface at angle smaller than the critical angle $\theta_c = \sin^{-1}\left(\frac{n_{vacuum}}{n_{BB}}\right) = \sin^{-1}\left(\frac{1}{n_{BB}}\right)$, will carry power into the space. By photon tunneling, the number of evanescent modes that carry extra energy into the object is [16]

$$N_{tunneling} = 4\pi\int_{\theta_c}^{\frac{\pi}{2}} d\theta_i \sin\theta_i \cos\theta_i T(\theta_i), \tag{5}$$

where transmissivity $T(\theta_i)$ is determined by [16]

$$T(\theta_i) = \begin{cases} \sec h^2(\alpha L), & \text{for } \alpha L<1 \\ \sin(2\xi_{12})\sin(2\xi_{23})\sec h^2(\alpha L), & \text{for } \alpha L>1 \end{cases} \tag{6}$$

In Eq. (6), α is the imaginary part of the evanescent wavevector

$$\alpha = \frac{\omega}{c}\sqrt{(n_{BB}\sin\theta_i)^2 - 1}, \tag{7}$$

and $\tan\xi_{12}^{TE} = \alpha/k_{1,z}$, $\tan\xi_{12}^{TM} = n_1^2\alpha/n_2^2 k_{1,z}$, $\tan\xi_{23}^{TE} = \alpha/k_{3,z}$, $\tan\xi_{23}^{TM} = n_3^2\alpha/n_2^2 k_{3,z}$.

3.2 Transfer Matrix Method for a Multilayered Structure

In Fig. 3(b), a multilayered structure is shown with semi-infinite top and bottom layers. Neglect absorption in all cases ($\mathrm{Im}(n_l)=\mathrm{Im}(\mu_l)=0$). The electric field is described as

$$E_l(z)=e^{ik_x x-i\omega t}\left(A_l e^{ik_{lz}z_l}+B_l e^{-ik_{lz}z_l}\right),\ l=2,3\cdots,N \tag{8}$$

where z_l is the relative z-direction coordinate measured from the top of the *lth* layer, A_l and B_l are the amplitudes at the interface for the "forward" and "backward" waves, respectively. According to the Snell's law, the x-direction wavevector is always

$$k_{lx}\equiv 2\pi n_l \sin\theta_1/\lambda\ . \tag{9}$$

And z-direction wavevectors are determined by

$$k_{lz}=\begin{cases}2\pi n_l\cos\theta_l/\lambda,\ \theta_l=\sin^{-1}\left(n_1\sin\theta_1/n_l\right), \text{ for propagating waves}\\ i\dfrac{2\pi}{\lambda}\sqrt{\left(n_1\sin\theta_1\right)^2-n_l^{\,2}}, |n_1\sin\theta|_1>|n_l|, \text{ for evanescent waves}\end{cases} \tag{10}$$

where for propagating waves k_{lz}<0 if n_l<0. This is due to a negative phase velocity in this case though the group velocity is pointing forward and negatively refracted [8, 12]. The forward evanescent waves will always exponentially decay, while the backward evanescent waves will grow exponentially. It should be noted that the discussed amplification of a near field is due to the multiple reflections inside a LHM, while for a single travel across the slab the rules for PIM still hold true.

The coefficients of adjacent layers are related by

$$\begin{pmatrix}A_l\\B_l\end{pmatrix}=P_l D_l^{-1}D_{l+1}\begin{pmatrix}A_{l+1}\\B_{l+1}\end{pmatrix}, \tag{11}$$

in which

$$P_1=\begin{pmatrix}1&0\\0&1\end{pmatrix},$$

$$P_l=\begin{pmatrix}e^{-ik_{lz}d_l}&0\\0&e^{ik_{lz}d_l}\end{pmatrix}, l=2,3\cdots \tag{12}$$

Define $\alpha_l=\dfrac{k_{lz}}{2\pi n_l/\lambda}$, $\beta_l=n_l/\mu_l$, and $\gamma_l=\alpha_l\beta_l$. The matrix D is expressed as

$$D_l=\begin{pmatrix}1&1\\\gamma_1&-\gamma_1\end{pmatrix}, \text{ for TE waves}$$

$$D_l=\begin{pmatrix}\alpha_l&\alpha_l\\\beta_l&-\beta_l\end{pmatrix}, \text{ for TM waves} \tag{13}$$

Following the chain rule, above equations yield

$$\begin{pmatrix}A_l\\B_l\end{pmatrix}=\left(\Pi_{l=1}^{N-1}P_l D_l^{-1}D_{l+1}\right)\begin{pmatrix}A_{l+1}\\B_{l+1}\end{pmatrix}. \tag{14}$$

Using B_N=0, the ratios $t=A_N/A_1$, $r=B_1/A_1$ can be determined. And the transmittivity and reflectivity are

$$T(\theta_1) = \mathrm{Re}\left(\frac{n_N \cos\theta_N}{n_1 \cos\theta_1}\right) tt^*, \text{ and } R = rr^* = 1 - T. \tag{15}$$

The field strength $|E|$ can be calculated by Eq. (8) in which $e^{ik_x x - i\omega t}$ is cancelled out when $|E|$ is normalized with the incident field strength $|E_i| = \left|e^{ik_x x - i\omega t}\right| |A_l + B_l|$.

3.3 Analysis of Photon Tunneling across a Vacuum Gap

Now we will consider a device with four layers from the top to the bottom: the heated blackbody, a vacuum (air) gap, a LHM layer, and an object layer. It can be proved that switching the second and third layers will not affect the overall transmissivity. However, separating the LHM layer from the blackbody is more practical.

Define $\alpha_{pq} = \frac{\alpha_p}{\alpha_q}$, $\beta_{pq} = \frac{\beta_p}{\beta_q}$, $\gamma_{pq} = \frac{\gamma_p}{\gamma_q}$. When $n_2 < n_1 \sin\theta_1 < n_4$, we have theoretical solutions for the transmission coefficient [13]

$$t = \begin{cases} \dfrac{4}{(1-\gamma_{21})(1+\gamma_{43})e^{\phi} + (1+\gamma_{21})(1-\gamma_{43})e^{-\phi}}, & \text{TE waves} \\ \dfrac{4}{(\beta_{21}-\alpha_{21})(\beta_{43}+\alpha_{43})e^{\phi} + (\beta_{21}+\alpha_{21})(\beta_{43}-\alpha_{43})e^{-\phi}}, & \text{TM waves} \end{cases} \tag{16}$$

Generally speaking, the transmissivity reaches its maximum under the condition $d_3 = d_2$, $n_3 = -n_2$, $\mu_3 = -\mu_2$, which indicates "anti-symmetric" geometry. In such a situation, the phase difference across medium 2 is compensated by the phase reversal in medium 3. Independent of θ_1, the transmissivity of evanescent waves is just one when $n_1 = n_4$, $\mu_1 = \mu_4$, $n_3 = -n_2$, $\mu_3 = -\mu_2$, and $d_3 = d_2$. The microscale radiative transfer will reach its theoretical limit for wavelengths associated with negative refraction, i.e., n_{BB}^2 times the spectral power density of a blackbody. By choosing object and blackbody materials with large n, we can obtain energy fluxes not achieved by any previous attempts.

To illustrate the enhanced tunneling effect, we calculate the transmissivity of typical waves as a function of $\frac{d_3 - d_2}{\lambda}$ and incident angles, similar to [13]. Since $\alpha d_2 > 10$ for fixed $d_2 = 2\lambda$ and selected incident angles, without the LHM layer the unachievable upper bound in Eq. (6) is approximately $4\exp(-2\alpha L)$ and is negligible. For $L = d_2 = 2\lambda$, $\theta_i = 80°$, the upper bound is 1.2×10^{-18}, while it is 4.86×10^{-11} for $\theta_i = 45°$. These values can also be observed at $\frac{d_3 - d_2}{\lambda} = -2$ in Fig. 4, which shows that adding an extra LHM layer will dramatically enhance the tunneling effect.

In current thermophotovoltaic devices, the gap L is still limited to tens of nanometers, which brings great difficulty to fabrications and also increase the product cost. Although our calculation shows the possibility of using much larger gap to achieve much higher energy fluxes, it should be noted that for large incident angles even a small deviation of

$\frac{d_3 - d_2}{\lambda}$ will cause a large reduction in T, which can be observed in Fig. 4. Furthermore, T is more sensitive to $\frac{d_3 - d_2}{\lambda}$ when n_1, n_4 are large. Although this is not good for thermophotovoltaic devices, this kind of sharp curves can be very useful in detecting the distance d_2 in the microscopy, in which we may be able to control the thickness d_3 to atomic or even subatomic level. Signal peaks are only observed when $|L - d_3| \ll \lambda$. This idea is similar to the Bragg reflection. The utilization of LHMs will dramatically increase the signal strength and also lead to a narrow observable $\frac{d_3 - d_2}{\lambda}$ width. The sensitivity will be greatly improved compared with conventional scanning photon tunneling microscopy, and the absolute value of required L can be enlarged with d_3.

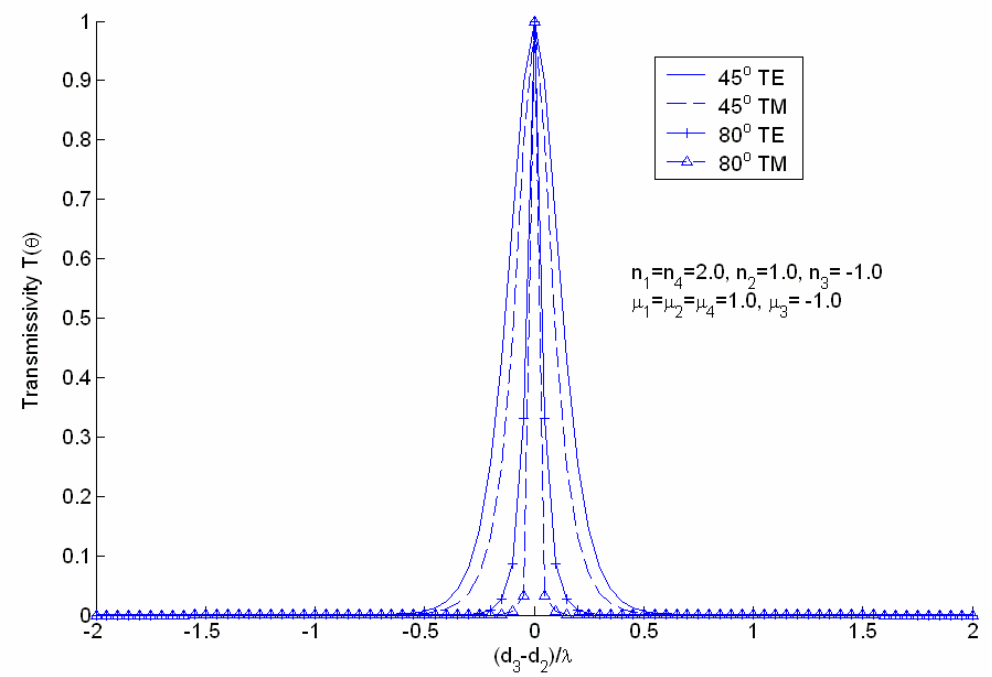

Fig. 4. Transmissivity as a function of $\frac{d_3 - d_2}{\lambda}$, $d_2 \equiv 2\lambda$.

Assuming TE and TM waves both account for half of the total radiative energy, Eq. (5) is integrated as a function of $\frac{d_3 - d_2}{\lambda}$ (Fig. 5). For $T(\theta_i)$, a singularity point occurs at $\theta_i = \theta_c$. When $\left|\frac{d_3 - d_2}{\lambda}\right| = 0$, the number of modes tunneling through the gap is 4.71, which is just the theoretical maximum $N = 4\pi \int_{\pi/6}^{\pi/2} \sin\theta_i \cos\theta_i d\theta_i = \frac{3}{2}\pi$. However, it

quickly drops to 0.12 when $\left|\frac{d_3 - d_2}{\lambda}\right| = 0.5$. In fabrications, the vacuum gap should be accurately adjusted so that the photon tunneling can be used to the fullest extent.

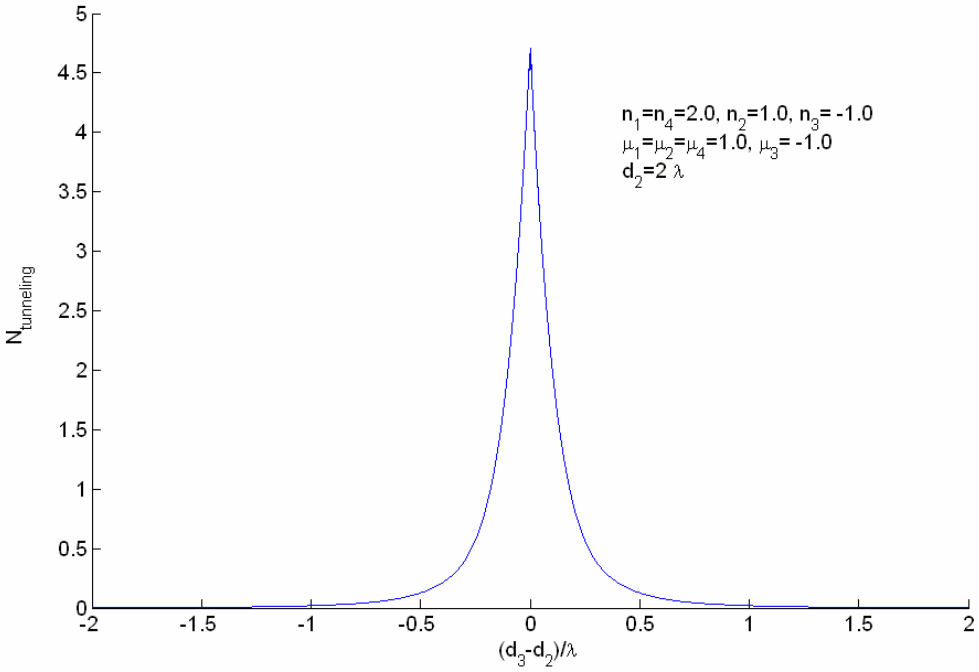

Fig. 5. $N_{tunneling}$ as a function of $\frac{d_3 - d_2}{\lambda}$, $d_2 \equiv 2\lambda$.

Figs. 6(a), (b) present the normalized TE evanescent field intensity across the vacuum and LHM layers. It is interesting that in both cases the maxima occur at the interface. For comparison, the cases replacing the LHM layer with vacuum are plotted in Figs. 7(a), (b). The field intensity will monotonously decay without a LHM layer. It should be noted that the field intensity variations in Fig. 6 is much higher than those in Fig. 7.

Our analysis is not only restricted to photon transports, but also applicable to other wavelike phenomena. Recently negative refraction for acoustic waves has been studied in 2D photonic crystals [18], so we may expect similar behavior, maybe unusual temperature profiles, existing within these structures. If we can make thin films of such photonic crystals with good thermal contacts, they may be useful in improving the current 3ω thermal conductivity measurements, which is also based on multilayered structures.

(a) 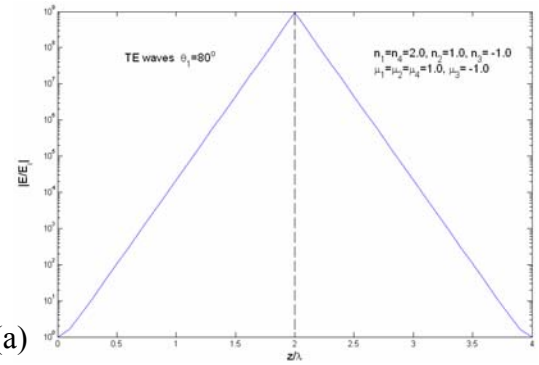

(b) 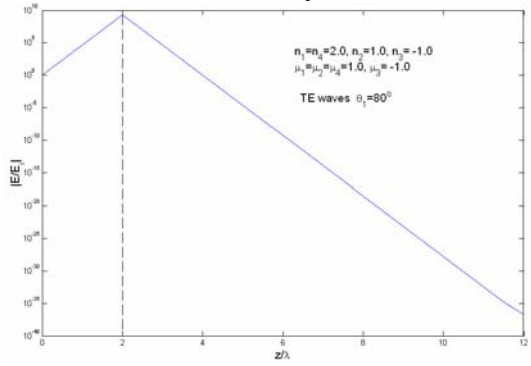

Fig. 6. The normalized TE evanescent fields in layer 2 and 3: (a) $d_2 = d_3 = 2\lambda$; (b) $d_2 = 2\lambda$, $d_3 = 12\lambda$. Dashed lines indicate the interface position.

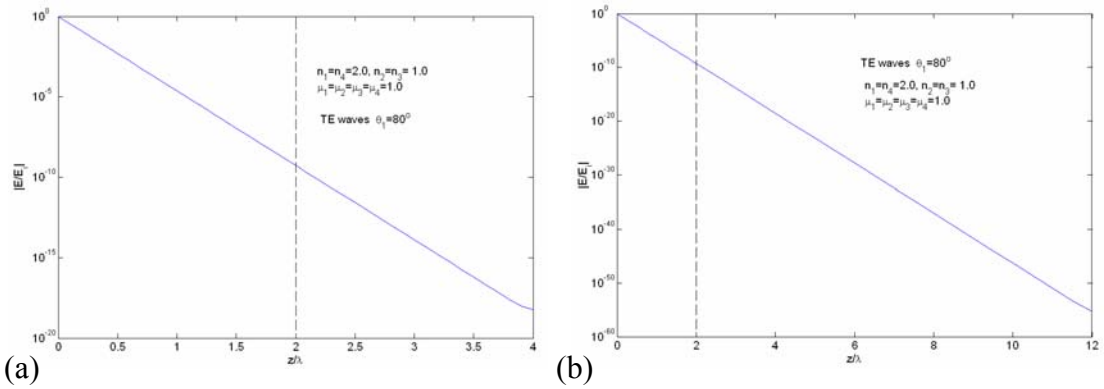

Fig. 7. Recalculation of Fig. 6 except for replacing the LHM layer with an extended vacuum gap.

3.4 Scanning Photon Tunneling Microscopy

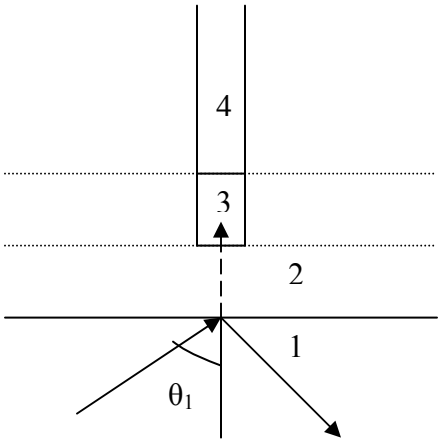

Fig. 8. Schematic diagram of unusual scanning photon tunneling microscopy

As discussed in the previous section, using a LHM layer will greatly improve the performance of the current scanning photon tunneling microscopy. The basic idea here is to add a LHM layer to the top of the probe (Fig. 8). The topography of the surface can be obtained by adjusting the tunneling signals to the largest at all scanned locations, which indicates a constant gap $L = d_3$ (or differed by a factor due to the finite cross section area of the probe) is maintained between the probe and the surface. This is similar to the constant-current mode of a scanning tunneling microscope. This method should be more accurate compared with that utilizing weak decaying evanescent waves. Since the boundary refraction on the sidewall of the probe must be considered, no simple theoretical solution is available for this 3D problem and it must be solved numerically. Therefore, here we will not compute the transmissivity but only demonstrate the idea.

4. Future Work

Although negative refraction promises to open up a variety of new applications, all current metamaterial samples tend to have significant losses, which greatly restrict their wide applications. Photonic crystals, which are periodic structures built on the scale of the optical wavelength, show the potential to overcome this difficulty [12, 17]. Using a photonic crystal consisting of a 2D square array of alumina rods, negative refraction has been observed for a gaussian beam [17]. Operating in the valence band to avoid the Bragg reflection, the transmission efficiency at a 13.7 GHz frequency has reached 63%. This transmission efficiency is almost three orders of magnitude larger than the typical transmission efficiency in a LHM. This effect may also be extended to optical wavelengths by using transparent semiconductors. Here we wonder whether it is possible to use an array of standing ZnO nanowires to realize similar functions. If so, this may reduce the current LHM size from millimeter level to nanoscale.

Since all current LHMs are anisotropic and confined to the microwave range, the impact will be enormous if an isotropic and homogeneous LHM can be realized in an optical frequency range. Recently it has been suggested that an atomic gas of three-level electro-magnetically induced transparency (EIT) system can be utilized to achieve this objective [19]. Based on quantum interference, the optical properties of the medium can be adjusted by a "coupling" laser beam at ultra low temperatures, which is utilized in the experiments of Bose-Einstein condensation [20]. Similar to the thermally controlled quantum dot (QD) optical gain [21], an approach to adjust the material property during operations will offer more flexibility to many applications.

5. Conclusion

In the history, the discovery of novel materials always boosted the development of technology. Similarly, we may expect a variety of technical innovations brought by LH materials, which can bend light in the "wrong" way. Unrestricted to waveguides, optical fibers, microwave filters, LH materials may play a very important role in the coming photonic era.

References:

1. V. G. Veselago, Sov. Phys. Usp. **10**, 509 (1968).
2. J. B. Pendry, Phys. Rev. Lett. **85**, 3966 (2000).
3. J. B. Pendry, A. J. Holden, D. J. Robbins, and W. J. Stewart, J. Phys.: Condens. Matter **10**, 4785 (1998).
4. D. R. Smith, W. J. Padilla, D. C. Vier, S. C. Nemat-Nasser, and S. Schultz, Phys. Rev. Lett. **84**, 4184 (2000).
5. R. A. Shelby, D. R. Smith, and S. Schultz, Science **292**, 79–81 (2001).
6. P. M. Valanju, R. M. Walser, and A. P. Valanju, Phys. Rev. Lett. **88**, 1874011–1874014 (2002).
7. N. Garcia and M. Nieto-Vesperinas, Opt. Lett. **27**, 885–887 (2002).
8. Z. M. Zhang, Keunhan Park, Journal of Heat Transfer **126**, 244 (2004).
9. C. G. Parazzoli, R. B. Greegor, K. Li, B. E. C. Koltenbah, and M. Tanielian, Phys. Rev. Lett. **90**, 1074011–1074014 (2003).
10. A. A. Houck, J. B. Brock, and I. L. Chuang, Phys. Rev. Lett. **90**, 1374011–1374014 (2003).

11. J. Pacheco, Jr., T. M. Grzegorczyk, B.-I. Wu, Y. Zhang, and J. A. Kong, Phys. Rev. Lett. **89**, 2574011–2574014 (2002).
12. S. Foteinopoulou, E. N. Economou, and C. M. Soukoulis, Phys. Rev. Lett. **90**, 1074021–1074024 (2003).
13. Z. M. Zhang and C. J. Fu, Applied Physics Letters **80**, 1097-1099 (2002).
14. J. B. Pendry, D. R. Smith, Physics Today **57**, 37 (2003).
15. N. Garcia1, and M. Nieto-Vesperinas, Phys. Rev. Lett. **88**, 207403-1 (2002).
16. J. L. Pan, H. K. H. Choy, and C. G. Fonstad, Jr., IEEE Trans. Electron Devices **47**, 241 (2000).
17. E. Cubukcu, K. Aydin, E. Ozbay, S. Foteinopoulou, C. M. Soukoulis, Nature **423**, 604 (2003).
18. X. Zhang, Z. Liu, Applied Physics Letters **85**, 341–343 (2004).
19. J. Shen, Z. Ruan, S. He, J. Zhejiang Univ Sci. **5**, 1322 (2004).
20. Lene Vestergaard Hau, S. E. Harris, Zachary Dutton, Cyrus H. Behroozi, Nature **397**, 594 - 598 (1999).
21. Gyoungwon Park, Oleg B. Shchekin, and Dennis G. Deppe, IEEE J. of Quantum Electronics **36**, 1065 (2000).